ISSN 1063-7842, Technical Physics, 2021, Vol. 66, No. 1, pp. 139–144. © Pleiades Publishing, Ltd., 2021.
Russian Text © The Author(s), 2021, published in Zhurnal Tekhnicheskoi Fiziki, 2021, Vol. 91, No. 1, pp. 145–151.

PHYSICAL ELECTRONICS

The Influence of the Thickness of Silicon- and Oxygen-Doped Hydrogenized Carbon Films on Their Surface Properties

A. S. Grenadyorov[a,*], A. A. Solov'ev[a], and K. V. Oskomov[a]

[a] *Institute of High-Current Electronics, Siberian Branch, Russian Academy of Sciences, Tomsk, 634055 Russia*

**e-mail: 1711Sasha@mail.ru*

Received July 15, 2020; revised July 15, 2020; accepted July 21, 2020

Abstract—Hydrogenized carbon films 0.5–7.0 μm thick doped with silicon (11.9 ± 0.4 at %) and oxygen (1.7 ± 0.1 at %) have been grown on VT-6 titanium and silicon substrates in an externally heated arc discharge plasma. The hardness, internal stresses, surface morphology, wettability, and surface potential of the films against their thickness have been studied. It has been found that as the film gets thicker, the allowable load on the material and its hardness grow. It has been shown that the films have low internal stresses (below 600 MPa) and the water contact angle is 75°–80°. It have turned out that an increase in film thickness raises the negative surface potential from 50 to 670 mV.

DOI: 10.1134/S1063784221010096

INTRODUCTION

Diamond-like carbon (a-C) and hydrogenized carbon (a-C:H) films are attracting much interest owing to their high hardness, low friction coefficient, high wear resistance, and biocompatibility [1]. Because of such a combination of properties, diamond-like films are in demand in medicine, mechanical engineering, aerospace engineering, and other branches of industry. However, diamond-like films have a significant drawback: high internal compression stresses (1.5–10.0 GPa), which, being due to a large content of sp^3 bonds, may cause cracking at high loads [2]. To reduce residual stresses in diamond-like films and improve the adhesion of the films, the following approaches are used: doping of films with different elements (N, Si, F, Cu, Ag, Mo, SiO_x, etc.) [3–7], application of an adhesive sublayer [8], high-temperature (>300°C) annealing [9], and electron and/or ion processing of films [10, 11].

Doping of hydrogenized carbon films with silicon (a-C:H:Si) or silicon dioxide (a-C:H:SiO_x) reduces internal stresses, raises adhesion, and improves the biomedical properties of films [12]. Hardness H of silicon-doped films drops to 10–20 GPa because of the decrease in the fraction of sp^3 hybridized carbon atoms. The properties of Si- or SiO_x-doped diamond-like films depend both on dopant concentration [13–15] and on deposition conditions (such as the amplitude of pulsed substrate bias [16, 17], composition and consumption of precursors [17, 18], and the density of ion current toward the substrate [19]).

When the silicon content in a-C:H:Si films rises from 4 to 16 at %, hardness H slightly drops (from 10.8 to 9.4 GPa) but adhesion improves considerably [13]. In this case, plasticity index H/E (E is the elasticity modulus) and plastic deformation resistance H^3/E^2 increase from 0.08 to 0.10 MPa and 65 to 100 MPa, respectively. In addition, the increase in silicon content in the film improves its biocompatibility [14]. It was shown [15] that when the silicon content in a-C:H:Si films rises from 0 to 22 at %, internal stresses decline from 1.5 to 1 GPa and the hardness decreases form 14 to 12 GPa.

In [16] it was shown that the tribological properties of a-C:H:SiO_x films obtained by plasma-assisted chemical vapor deposition depend on the amplitude of rf substrate bias voltage. At an optimal bias voltage of −100 V, the films had a low friction coefficient (less than 0.05) and a high adhesive strength (a critical load at scratch tests was equal to 32 N). In [7], the hardness of the film was varied between 5 and 17 GPa depending on bias voltage and precursor (hexamethyldisiloxane) consumption.

It was found [20] that the mechanical performance of a-C:H films, as well as their tribological properties, are thickness dependent. The hardness of 1.6- and 2.4-μm-thick films was equal to 24 and 33 GPa, respectively, with wear rates being close to each other. This means that thicker films will serve for a longer time under identical conditions. However, the thickness dependence of silicon- and oxygen-doped a-C:H films has been little understood to date. In [21], the contact angle of wetting for a-C:H:SiO_x films from 4 to 180 nm in thickness was measured. This angle depends on thickness only slightly and varies between 67° and 76°. In [22], hardness H and elasticity modulus E of

films 2–9 μm thick were measured. It turned out that H and E vary insignificantly in this thickness range, being equal to 22–25 and 135–140 GPa, respectively.

Owing to a unique set of mechanical, tribological, and biomedical (biocompatibility) properties, diamond-like films are of great interest in medicine, in which they can be used as wear-resistant and barrier coatings for metallic implants. Medical implants are usually fabricated of stainless steel, as well as titanium- and cobalt-based alloys. Electrical compatibility between implants and living tissues is a critical characteristic for their interaction [23]. Electric fields in tissues govern the migration [24] and vitality of cells. It is known that blood cells have a negative zeta-potential [25].; therefore, to prevent blood cells from adhering to the implant surface, its potential must also be negative. In the case of dielectrics, the surface electrostatic potential is due to the self-charge and/or a charge resulting from external actions.

The aim of this study was to see how the thickness of a-C:H:SiO_x films applied from the externally heated arc discharge plasma influences the morphology, mechanical performance, and electrostatic potential of a surface being modified.

1. EXPERIMENTAL

As substrates, we used 15 × 15-mm square plates of VT-6 titanium, 0.2-mm thick (average roughness R_a about 0.25 μm and 400-μm-thick Si(100) wafers (R_a less than 0.015 μm). Experiments were conducted mainly with VT-6 substrates; sometimes, however, silicon substrates were used for convenience or to improve the measurement accuracy (for example, in internal stress measurements). Substrates were cleaned in an ultrasonic bath, which was filled first with isopropyl alcohol, then with acetone, and finally with distilled water. In each of the liquids, substrates were cleaned for 10 min. After that, substrates were dried in a compressed air flow. The working chamber was evacuated to a residual pressure of 10^{-2} Pa by means of a turbomolecular pump. The block diagram and parameters of the experimental setup were described in detail elsewhere [19].

To reduce the surface roughness, VT-6 substrates were subjected to electron-beam processing (EBP) [26]. To this end, a pulsed low-energy high-current electron beam with an energy density of 6.5 J/cm^2 and a number of pulses of 10 was applied. After EBP, the surface roughness R_a decreased from 0.25 to 0.15 μm. Before an a-C:H:SiO_x film was deposited, substrates were processed in an argon plasma at a pressure of 0.3 Pa for 10 min to remove oxide inclusions from the surface. In this case, a bipolar bias voltage with a negative voltage pulse of 1000 V, a voltage frequency of 100 kHz, and a fill factor of 60% was applied to the substrate holder. The discharge current and voltage were, respectively, 7.0 ± 0.5 A and 100 ± 5 V, and the heating current of the tungsten cathode was 45 ± 5 A. Then, an a-C: H: SiO_x film was deposited from a mixture of argon and polyphenyl methylsiloxane (PPMS) vapor. The argon flow rate was 4 ± 0.2 L/h, and that of PPMS was 1.0 ± 0.1 mL/h. The working pressure was equal to 0.1 Pa, and a bias voltage with a negative pulse amplitude of 300 V was applied to the substrate holder. The discharge current and voltage were, respectively, 5.0 ± 0.2 A and 140 ± 5 V, and the heating current of the tungsten cathode was 45 ± 5 A. The temperature of the substrate holder during deposition was no higher than 200°C. The film growth rate was 19 ± 1 nm/min.

The surface of obtained substrates was examined using a QUANTA 200 scanning electron microscope (FEI Co., United States). Micrographs were taken at an accelerating voltage of 30 kV, and the elemental composition was determined at a voltage of 10 kV. Micrographs were processed by means of the ImageJ 1.5 program package. Internal stresses in the film were determined by measuring the curvature of a 20 × 2 × 0.44-mm silicon sample before and after the application of the a-C:H:SiO_x film. The surface curvature was measured using a Micro Measure 3D Station three-dimensional contactless profilometer (STIL, France). Internal stresses were calculated by the Stoney formula [27]. The contact angle of wetting for water was determined by a KRÜSS Easy Drop device. In each sample, the contact angle was measured three times and then the average value was found. The values of H and E were determined using a Nanotest 600 instrument (Micro Materials Ltd., United Kingdom) by the Oliver–Pharr method [28]. The indentation load was varied between 10 and 100 mN. Parameters H and E were measured 10 times, after which the average value was found. The adhesion strength of the film was mentioned by an MST-S-AX-0000 microscratch tester (CSEM, Switzerland). A diamond needle with a tip radius of 100 μm was moved over the film surface at a constant rate of 2.45 mm/min with load gradually increasing with a rate of 3.75 N/min. The maximal applied load was equal to 15 N, and the scratch length was 7 mm. The surface roughness and electrostatic potential of samples were determined using a Solver HV tapping-mode atomic force microscope (NT-MDT, Zelenograd, Russia) with a cantilever made of W_2C. Experimental data were processed by means of the Gwiddion program package. The surface potential was found by the Kelvin method [29].

2. RESULTS AND DISCUSSION

Figure 1 shows the micrographs of the a-C:H:SiO_x film applied on the VT-6 substrate. It is known that the surface roughness of amorphous diamond-like coatings is low (0.2–2.0 nm) [30]. Therefore, the surface morphology of coated samples to a great extent depends on that of the substrate. At a small thickness of coatings, they copy the surface relief of substrates. As coatings get thicker, the film is expected to smooth

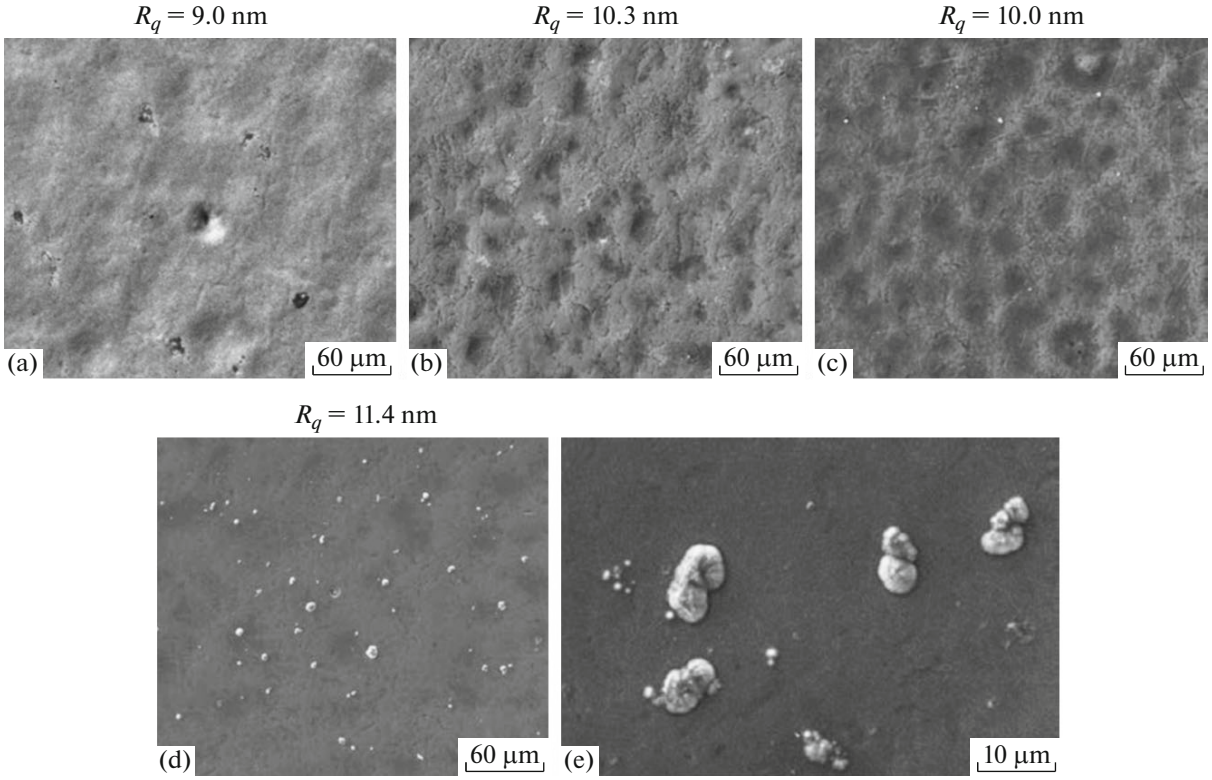

Fig. 1. Surface images of a-C:H:SiO_x films with a different thickness applied on VT-6 titanium substrates: (a) uncovered substrate; (b–d) films 1.7, 4.6, and 7.5 μm thick, respectively; and (e) magnified image of the 7.5-μm-thick film.

out. The micrograph in Fig. 1a is the surface image of the titanium substrate after EBP. EBP alters the surface layer structure through dynamic recrystallization, which is initiated by superhigh heating and cooling rates. Depressions and microcraters may be observed on the sample surface. Their number can be minimized by appropriately selecting EBP conditions [31]. In Fig. 1b it is seen that depressions appear on the surface of the 1.7-μm-thick a-C:H:SiO_x film, which persist even after EBP. They become less visible on the surface of the 4.6-μm-thick film (Fig. 1c) and completely disappear on the surface of the 7.5-μm-thick film (Fig. 1d).

According to energy-dispersive analysis data, the films contain 83 ± 1 at % of carbon, 11.9 ± 0.4 at % of silicon, 1.7 ± 0.1 at % of oxygen, and 3.2 ± 0.3 at % of argon. It seems that argon present in the film results from argon ion bombardment of the film during growth. The surface of the 7.5-μm-thick film contains intricately shaped particles to 9 μm across (Fig. 1 e). A follows from energy-dispersive analysis data, these particles contain about 32 at % of silicon, which far exceeds the content of silicon in films. More detailed examination of a-C:H:SiO_x films by means of X-ray photoelectron spectroscopy, Raman spectroscopy, and IR spectroscopy is presented in our previous articles [31, 32].

According to atomic force microscopy (AFM) data, root-mean-square surface roughness R_q of the samples is 10 ± 1 nm over a 5 × 5-μm^2 area.

Figure 2 shows the thickness dependences of internal stresses σ and contact angle of wetting θ. It was found that internal stresses in a-C:H:SiO_x films are compressive stresses. When the thickness increases from 1.7 to 7.5 μm, internal stresses rise from 410 to 530 MPa. Nevertheless, these values are far below those typical of diamond-like films. Even 1-μm-thick-C:H:SiO_x films obtained in [17] had higher internal stresses: 0.5–1.4 GPa depending on substrate bias voltage and hexamethyldisiloxane consumption.

A clear-cut dependence of the contact angle on a-C:H:SiO_x film thickness is not observed (Fig. 2). For the films being studied, the contact angle varies between 74° and 79°. Similar values of contact angle (75°–78°) for a-C:H:SiO_x films were obtained in [33]. The absence of the thickness dependence of contact angle comes as no surprise, since the surface wettability depends on the chemical composition of the film and the presence of polar groups on its surface, which does not depend on thickness.

Figure 3 plots the hardness versus indentation load in the load interval 10–100 mN for VT-6 titanium substrates coated by a-C:H:SiO_x films with different thicknesses. When the load in the uncoated sample

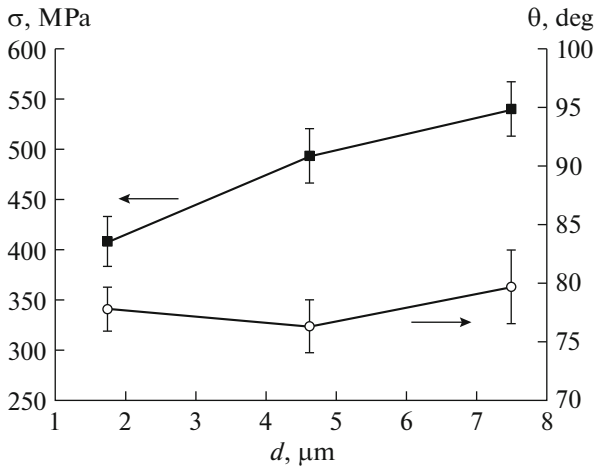

Fig. 2. Internal stresses σ and contact angle of wetting θ vs. a-C:H:SiO_x film thickness.

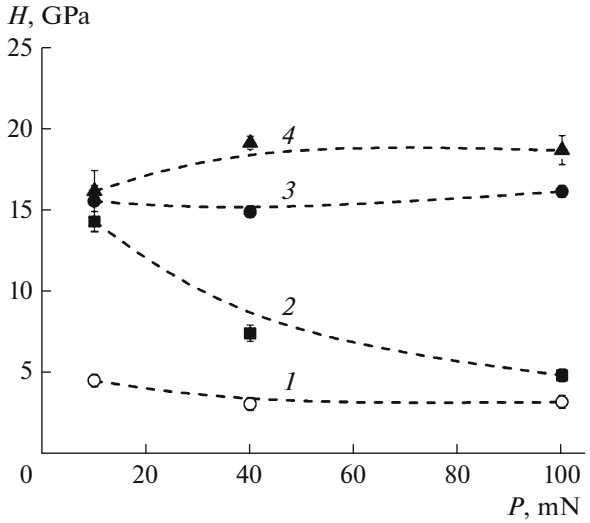

Fig. 3. Hardness *H* vs. load *P* on the indenter for (*1*) VT-6 titanium substrate and a-C:H:SiO_x films (*2*) 1.7, (*3*) 4.6, and (*4*) 7.5 μm in thickness.

rises from 10 to 100 mN, the hardness drops from 4.5 to 3.0 GPa (Fig. 3, curve *1*). After the application of a 1.7-μm-thick a-C:H:SiO_x film, the surface hardness increases threefold (to 14.3 GPa) at a load of 10 mN. In this case, the indenter penetration depth equals 162 nm. For a load of 100 mN, the hardness lowers to 4.8 GPa because of the influence of the less hard substrate. It is known that the actual hardness of the film can be measured if the penetration depth is not greater than 10% of the film thickness [34]. At loads of 40 and 100 mN, the penetration depths were 550 and 1100 nm, respectively. Then, for an a-C:H:SiO_x film 1.7 μm thick, it is reasonable to measure hardness only at a load of 10 mN. At a load of 10 mN, the hardness of a 4.6-μm-thick film is 15.6 GPa, and the increase in load to 100 mN decreases hardness insignificantly. This means that the substrate influences the measured values of hardness to a lesser extent. The indenter penetration depth at a load of 100 mN equals 550 nm. After the a-C:H:SiO_x film 7.5 μm thick was applied, the surface hardness in the given load interval even somewhat increases (Fig. 3, curve *4*). At a load of 40 mN, the hardness was equal to 19.2 GPa (with an indenter penetration depth of 342 nm). It seems that the substrate influences hardness measurements even if the penetration depth does not exceed 10% of the film thickness.

Table 1. Mean surface potential of a-C:H:SiO_x films vs. thickness

Film thickness, μm	Surface potential, mV	
	Si-substrate	VT-6 titanium substrate
0.1	−48.2	−65.9
1	−280	−210.9
4	−520.1	–
7	−676.7	–

Figure 4 shows scratch (hardness) test data for the a-C:H:SiO_x films, namely, signals from an acoustic emission sensor and scratch images at different loads on the indenter. According to acoustic emission data, the maximal critical load at which the coating breaks down is observed in the thinnest film (1.7 μm). The critical load for this film was equal to 13 N. As the thickness of this film increases from 4.6 to 7.5 μm, the critical load declines to 9 N.

The electrostatic field potential on the surface of a-C:H:SiO_x films was measured by the double pass method using a Kelvin-probe atomic force microscope. In the first pass, the surface relief of the sample was determined in the tapping mode. In the second pass, this relief was monitored by passing at some height above the sample to determine the surface electrostatic potential. It was found that the surface potential of a-C:H:SiO_x films applied on silicon and VT-6 substrates is negative (Table 1). Remarkably, when the thickness of films on Si substrates grows from 0.5 to 7.0 μm, the mean value of surface potential grows (in magnitude) from −50 to 670 mV. The potential of films applied on VT-6 substrates has comparable values and also tends to grow with film thickness.

As follows from energy-dispersive analysis data, the elemental composition of the film does not change with increasing film thickness. Accordingly, the permittivity of the film is thickness independent. This means that the surface potential is influenced by the capacitance of the dielectric, which is inversely proportional to the thickness of the of a-C:H:SiO_x film.

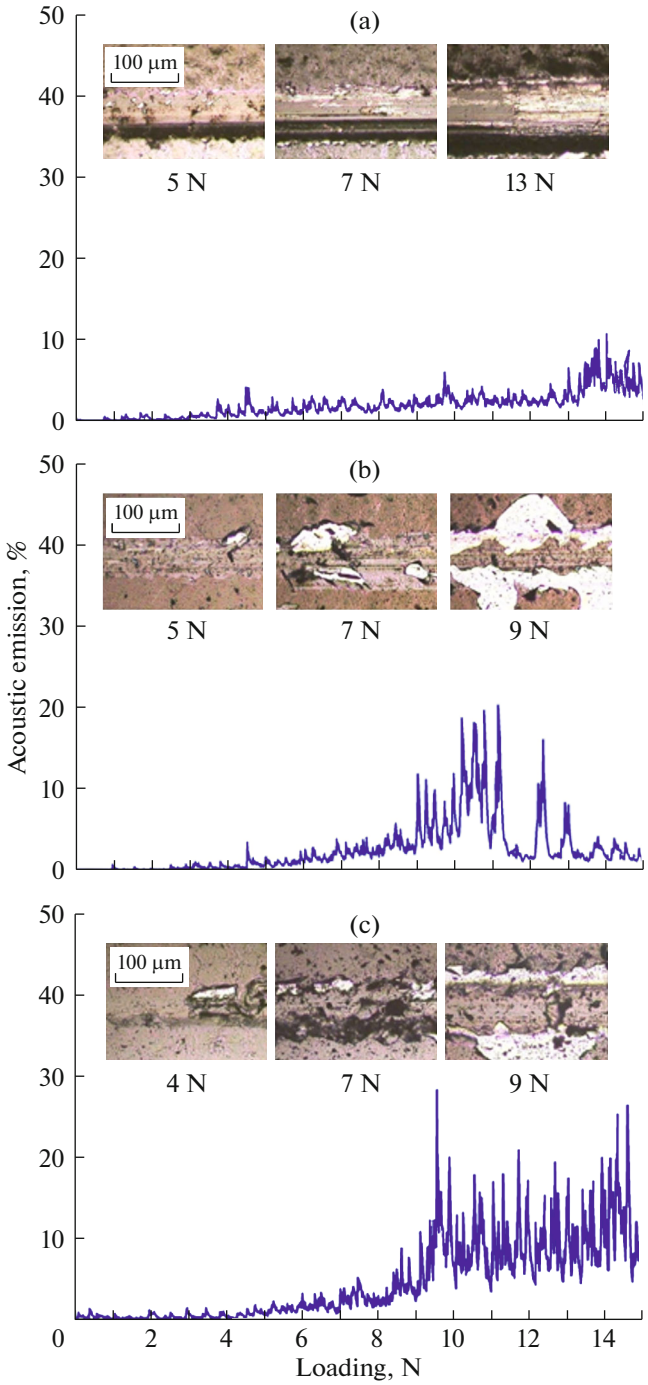

Fig. 4. Acoustic emission signals and scratch images taken during scratch testing of a-C:H:SiO_x films (a) 1.7, (b) 4.6, and (c) 7.5 μm in thickness.

CONCLUSIONS

The influence of the thickness of silicon-doped (11.9 ± 0.4 at %) and oxygen-doped (1.7 ± 0.1 at %) hydrogenized carbon films (obtained in the externally heated arc discharge plasma) on their surface morphology, hardness, internal stresses, adhesion, and surface electrostatic potential was studied. It was shown that the increase in the thickness of a-C:H:SiO_x films in the interval 1.7–7.5 μm smoothes out the surface roughness on VT-6 titanium substrates. Although internal compressive stresses rise from 400 to 550 MPa when a-C:H:SiO_x films thicken, these values are much lower than in undoped diamond-like films. The application of a-C:H:SiO_x films on VT-6 titanium substrates increases the hardness of the films, and the increase in their thickness raises the allowable load on the material. This is of importance when the films are used as protective or wear-resistant coatings. It was found that when a-C:H:SiO_x films thicken, their negative surface potential grows from 50 to 670 mV. This fact is significant when these films are used in fabrication of medical products and implants to be in contact with blood.

ACKNOWLEDGMENTS

The authors thank the administration of the Tomsk Regional Research Center for Collective Use center (Siberian Branch, Russian Academy of Sciences) for the submission of the NanoTest 600 nanoindenter.

FUNDING

This study was supported by grant no. MK-1234.2020.8 of the President of the Russian Federation. Surface potential measurements were supported by the Russian Science Foundation, grant no. 19-19-00186.

CONFLICT OF INTEREST

The authors declare that they have no conflicts of interest.

REFERENCES

1. X. An, Zh. Wu, L. Liu, T. Shao, S. Xiao, S. Cui, H. Lin, R. K. Y. Fu, X. Tian, P. K. Chu, and F. Pan, Surf. Coat. Technol. **365**, 152 (2019). https://doi.org/10.1016/j.surfcoat.2018.08.099
2. C. W. Zou, H. J. Wang, L. Feng, and S. W. Xue, Appl. Surf. Sci. **286**, 137 (2013). https://doi.org/10.1016/j.apsusc.2013.09.036
3. D. C. Sutton, G. Limbert, D. Stewart, and R. J. K. Wood, Friction **1** (3), 210 (2013). https://doi.org/10.1007/s40544-013-0023-1
4. R. Paul, S. Bhattacharyya, R. Bhar, and A. Pal, Appl. Surf. Sci. **257**, 10451 (2011). https://doi.org/10.1016/j.apsusc.2011.06.144
5. W. Yue, X. Gao, C. Wang, Z. Fu, X. Yu, and J. Liu, Mater. Lett. **73**, 202 (2012). https://doi.org/10.1016/j.matlet.2012.01.044
6. X. Li, P. Ke, and A. Wang, AIP Adv. **5** (1), 017111 (2015). https://doi.org/10.1063/1.4905788
7. H. W. Choi, R. H. Dauskardt, S.-C. Lee, K.-R. Lee, and K. H. Oh, Diamond Relat. Mater. **17**, 252 (2008). https://doi.org/10.1016/j.diamond.2007.12.034

8. K.-R. Lee, K. Y. Eun, I. Kim, and J. Kim, Thin Solid Films **377**–**378**, 261 (2000). https://doi.org/10.1016/S0040-6090(00)01429-2

9. Abdul Wasy Zia, Zhifeng Zhou, Po Wan Shum, and Lawrence Kwok Yan Li, Surf. Coat. Technol. **320**, 118 (2017). https://doi.org/10.1016/j.surfcoat.2017.01.089

10. P. A. Karaseov, O. A. Podsvirov, K. V. Karabeshkin, A. Ya. Vinogradov, A. Azarov, A. I. Titov, and A. S. Smirnov, Nucl. Instrum. Methods Phys. Res., Sect. B **268**, 3107 (2010). https://doi.org/10.1016/j.nimb.2010.05.063

11. M. Shiureviciute, J. Laurikaitiene, D. Adliene, L. Augulis, Z. Rutkuniene, and A. Jotautis, Vacuum **83**, s159 (2009). https://doi.org/10.1016/j.vacuum.2009.01.052

12. K. Koshigan, F. Mangolini, J. B. McClimon, B. Vacher, S. Bec, R. W. Carpick, and J. Fontaine, Carbon **93**, 851 (2015). https://doi.org/10.1016/j.carbon.2015.06.004

13. D. Bociaga, A. Sobczyk-Guzenda, W. Szymanski, A. Jedrzejczak, A. Jastrzebska, A. Olejnik, and K. Jastrzebski, Appl. Surf. Sci. **417**, 23 (2017). https://doi.org/10.1016/j.apsusc.2017.03.223

14. D. Bociaga, M. Kaminska, A. Sobczyk-Guzenda, K. Jastrzebska, L. Swiatek, and A. Olejnik, Diamond Relat. Mater. **67**, 41 (2016). https://doi.org/10.1016/j.diamond.2016.01.025

15. A. Bendavid, P. J. Martin, C. Comte, E. W. Preston, A. J. Haq, F. S. Magdon Ismail, and R. K. Singh, Diamond Relat. Mater. **16**, 1616 (2007). https://doi.org/10.1016/j.diamond.2007.02.006

16. N. Kumar, S. A. Barve, S. S. Chopade, K. Rajib, N. Chand, D. Sitaram, A. K. Tyagi, and D. S. Patil, Tribol. Int. **84**, 124 (2015). https://doi.org/10.1016/j.triboint.2014.12.001

17. D. Batory, A. Jedrzejczak, W. Szymanski, P. Niedzielski, M. Fijalkowski, P. Louda, I. Kotela, M. Hromadka, and J. Musil, Thin Solid Films **590**, 299 (2015). https://doi.org/10.1016/j.tsf.2015.08.017

18. A. S. Grenadyorov, K. V. Oskomov, N. F. Kovsharov, and A. A. Solovyev, J. Phys.: Conf. Ser. **1115**, 042046 (2018). https://doi.org/10.1088/1742-6596/1115/4/042046

19. A. S. Grenadyorov, A. A. Solovyev, K. V. Oskomov, and V. O. Oskirko, J. Vac. Sci. Technol., A **37** (6), 061512 (2019). https://doi.org/10.1116/1.5118852

20. F. F. Conde, J. A. Á. Diaz, G. F. da Silva, and A. P. Tschiptschin, Mater. Res. **22** (2), e20180499 (2019). https://doi.org/10.1590/1980-5373-mr-2018-0499

21. S. Meškinis, S. Tamulevičius, V. Kopustinskas, M. Andrulevičius, A. Guobienė, R. Gudaitis, and I. Liutvinienė, Thin Solid Films **515** (19), 7615 (2007). https://doi.org/10.1016/j.tsf.2006.11.089

22. E. V. Zavedeev, O. S. Zilova, A. D. Barinov, M. L. Shupegin, N. R. Arutyunyan, B. Jaeggi, B. Neuenschwander, and S. M. Pimenov, Diamond Relat. Mater. **74**, 45 (2017). https://doi.org/10.1016/j.diamond.2017.02.003

23. I. A. Khlusov, V. F. Pichugin, E. A. Gostischev, Yu. P. Sharkeyev, R. A. Surmenev, M. A. Surmeneva, Y. V. Legostayeva, M. V. Chaikina, M. V. Dvornichenko, and N. S. Morozova, Byull. Sibir. Med. **10** (3), 72 (2011). https://doi.org/10.20538/1682-0363-2011-3-72-81

24. M. Zhao, B. Song, J. Pu, T. Wada, B. Reid, G. Tai, F. Wang, A. Guo, P. Walczysko, Yu Gu, T. Sasaki, A. Suzuki, J. V. Forrester, H. R. Bourne, P. Devreotes, C. Mccaig, and J. M. Penninger, Nature **442** (7101), 457 (2006). https://doi.org/10.1038/nature04925

25. O. V. Bondar, D. V. Saifullina, I. I. Shakhmaeva, I. I. Mavlyutova, and T. I. Abdullin, Acta Nat. **4** (1), 78 (2012). https://doi.org/10.32607/20758251-2012-4-1-78-81

26. V.P. Rotstein, R. Gyuntsel, A.B. Markov, D.I. Proskurovsky, M.T. Fam, E. Rikhter, and V.A. Shulov, Fiz. Khim. Obr. Mater. **1**, 62 (2006).

27. J. B. Cai, X. L. Wang, W. Q. Bai, X. Y. Zhao, T. Q. Wang, and J. P. Tu, Appl. Surf. Sci. **279**, 450 (2013). https://doi.org/10.1016/j.apsusc.2013.04.136

28. W. C. Oliver and G. M. Pharr. J. Mater. Res. **19** (1), 3 (2004). https://doi.org/10.1557/jmr.2004.19.1.3

29. V. A. Novikov, D. V. Grigoryev, A. V. Voitsekhovskii, S. A. Dvoretsky, and N. N. Mikhailov, J. Surf. Invest.: X-Ray, Synchrotron Neutron Tech. **10** (5), 1096 (2016). https://doi.org/10.1134/S1027451016050372

30. X. L. Peng, Z. H. Barber, and T. W. Clyne, Surf. Coat. Technol. **138**, 23 (2001). https://doi.org/10.1016/S0257-8972(00)01139-7

31. A. S. Grenadyorov, A. A. Solovyev, K. V. Oskomov, S. A. Onischenko, A. M. Chernyavskiy, M. O. Zhulkov, and V. V. Kaichev, Surf. Coat. Technol. **381**, 125113 (2020). https://doi.org/10.1016/j.surfcoat.2019.125113

32. A. S. Grenadyorov, A. A. Solovyev, K. V. Oskomov, and V. S. Sypchenko, Surf. Coat. Technol. **349**, 547 (2018). https://doi.org/10.1016/j.surfcoat.2018.06.019

33. A. A. Ogwu, T. I. T. Okpalugo, and J. A. D. McLaughlin, AIP Adv. **2** (3), 032128 (2012). https://doi.org/10.1063/1.4742852

34. A. R. Shugurov, A. V. Panin, and K. V. Oskomov, Phys. Solid State **50** (6), 1050 (2008). https://doi.org/10.1134/S1063783408060097

Translated by V. Isaakyan